Proc. Natl. Acad. Sci. USA
Vol. 96, pp. 1206–1211, February 1999
Geophysics

This contribution is part of the special series of Inaugural Articles by members of the National Academy of Sciences elected on April 28, 1998.

Separation of a midlevel density current from the bottom of a continental slope

M. E. STERN*

Department of Oceanography, Florida State University, Tallahassee, FL 32306-4320

Contributed by M. E. Stern, December 14, 1998

ABSTRACT **The high-salinity water flowing out of the Mediterranean Sea descends to mid depths in the density-stratified ocean, continues as a narrow jet along the Iberian continental slope, and intermittently detaches large-scale eddies (called "Meddies"). This process is important because it maintains the relatively high mean salinity of a major water mass (the "Mediterranean Intermediate Water") in the North Atlantic. Our simplified model of this jet consists of a moving layer with intermediate density ρ_2 sandwiched between motionless layers of density $\rho_1 < \rho_2$ and $\rho_3 > \rho_2$. The inshore (anticyclonic) portion of the midlevel jet (in the "ρ_2-water") rests on an inclined bottom (the continental slope), whereas the (cyclonic) offshore portion rests on the density interface of the stagnant deep (ρ_3) layer. An inviscid, *steady*, and finite-amplitude longwave theory is used to show that if the cross-stream topographic slope *increases* gradually in the downstream direction, then the "ρ_2-jet" is deflected off the bottom slope and onto the upper density interface of the ρ_3 layer. The computed magnitude of this separation effect is such as to produce an essentially free jet which is removed from the *stabilizing* influence of the continental topography. It is therefore conjectured that time-dependent effects (baroclinic instability) will produce further amplification, causing an eddy to detach seaward from the branch of the jet remaining on the slope.**

Section 1. Introduction

The lateral separation from the continental slope of large-scale currents such as the Gulf Stream and the Mediterranean Outflow Current is an important oceanographic process, but there are significant differences between these two types. After the Gulf Stream emerges from the Straits of Florida the inshore (cyclonic half) of the jet extends from the bottom of the continental slope to the top of the ocean. As the jet progresses northward the water lying over the continental slope is gradually displaced off the slope and onto isopycnal surfaces. The separation from the continental slope is virtually complete at Cape Hatteras, North Carolina, at which point the Gulf Stream is essentially a *free* jet removed from restraining topography. While many large-scale factors enter into the dynamics of the Gulf Stream, it has been suggested (1) that the separation of the inshore half is an inertial process (conservation of potential vorticity), and one that can be explained by the net downstream increase of the cross-stream bottom slope, such as is observed (2) upstream of Cape Hatteras. The dynamical significance of the formation of such a free jet lies in the fact that it is much more unstable than a boundary jet that is under the restraining influence of sloping bottom topography; consequently wave amplitudes increase greatly downstream of Cape Hatteras, as is commonly observed in infrared satellite images of ocean temperatures. In midocean these waves in the Gulf Stream become so large that they "pinch off" from the main jet and deposit their thermal anomalies on either side, thereby initiating the process by which the heat transport of the semipermanent oceanic gyres is mixed in the surrounding water mass.

The Mediterranean Outflow Jet (Fig. 1), on the other hand, is a subsurface current flowing along the Iberian continental slope, and it will be modeled by a highly simplified vertical section (Fig. 2) consisting of only three density layers. Especially noteworthy in Fig. 1 is the fact that the jet following the topographic isobaths along the Iberian coast *intermittently* detaches eddies seaward (3), while the remaining portion of the jet continues along the slope until its temperature and salinity anomalies are entirely "diluted" in this manner.

Eddies form in a similar way elsewhere in the world ocean. D'Asaro (4, 5) reported a smaller-sized anticyclone at midlevels in the Arctic. Although it formed earlier than when observed and more remotely, the formation was attributed to the flow around a sharp coastal corner. This classical kind of boundary layer separation effect also occurs in laboratory experiments (6, 7) when a *rotating density* current flows along a vertical wall towards a sharp corner; if this makes an obtuse angle greater than 45° + 180°, then an eddy detaches from the boundary. The sharp corner, however, plays an inordinately large role, since separation does not occur at a continuously curved vertical wall if the radius of curvature exceeds the value of the typical current divided by the Coriolis parameter f (7). Since such a large radius of curvature is not typical of the relevant Iberian isobaths, it is probable that the downstream variation in cross-stream bottom slope is a more important topographic factor in the formation of meddies. Bower *et al*. (3) have measured the paths of floats placed in the stream (Fig. 1C), and although these are highly variable in space and time these authors indicate that some aspect of the topography is a controlling factor.

The role of topographic slope for eddy formation and separation appears in many numerical model studies. Jiang and Garwood (8) have computed the descent of a density current on a *uniformly* sloping bottom into continuously stratified ambient fluid. When the plume reaches its own density level it turns and flows parallel to the isobaths as an essentially laminar jet—i.e., no strong instability eddies occur, and there is no boundary layer separation. This illustrates the fact that the uniform bottom slope (relative to the ambient density surfaces) greatly reduces the amplitude of instability waves, such as occur in a *free* jet. In the latter case, numerical calculations (9) have been made for the California Coastal

PNAS is available online at www.pnas.org.

*e-mail: stern@ocean.fsu.edu.

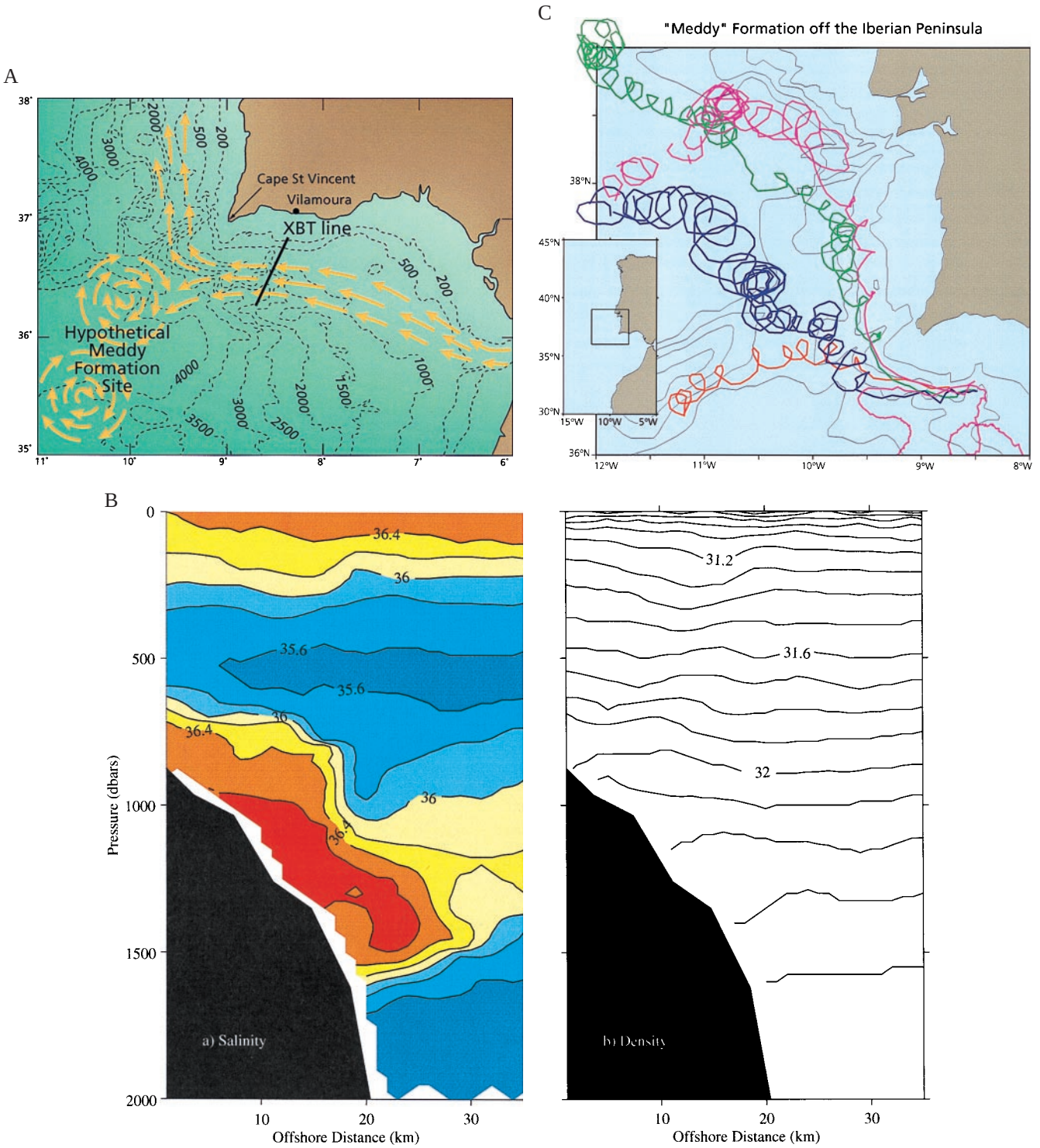

FIG. 1. (*A*) Schematic diagram [courtesy of Jack Cook/Woods Hole Oceanographic Institution (WHOI) Graphics] of the Mediterranean outflow current along the Iberian continental slope [isobaths (in meters) dashed], and the intermittent detachment of "meddies" at a depth of ≈1 km. These relatively salty and warm eddies lie above denser water in the Atlantic Ocean. The XBT line of temperature measurements. (*B*) A vertical cross section (courtesy of Amy Bower/WHOI) of salinity isolines (*a*) (looking into the stream) and corresponding density isolines (*b*), which qualitatively indicate the high salinity (>36 parts per thousand) outflow and the gravitationally stable density field (increasing downwards). One dbar = 10^4 Pa. (*C*) Long time trajectories of neutral floats (courtesy of Amy Bower/WHOI) placed in the high-salinity core (*B*). Some floats occasionally detach from the main core and rotate clockwise in the anticyclonic meddies, while the remainder of the jet continues along the isobaths. Eventually all of the high-salinity core is "detrained" and replaced by Atlantic water.

Current at a time when it was relatively far from the continental slope, in which instance the initial unstable equilibrium jet rapidly developed eddies that pinched off on either side. Similar results for the Mediterranean Outflow Current, but with topography removed, have been obtained (10). Unanswered, however, is the question of the mechanism for removing the current from the influence of the coastal topography and for creating the unstable initial state. This question has been addressed (11) by using a primitive three-dimensional baroclinic model in a large computational domain, wherein the

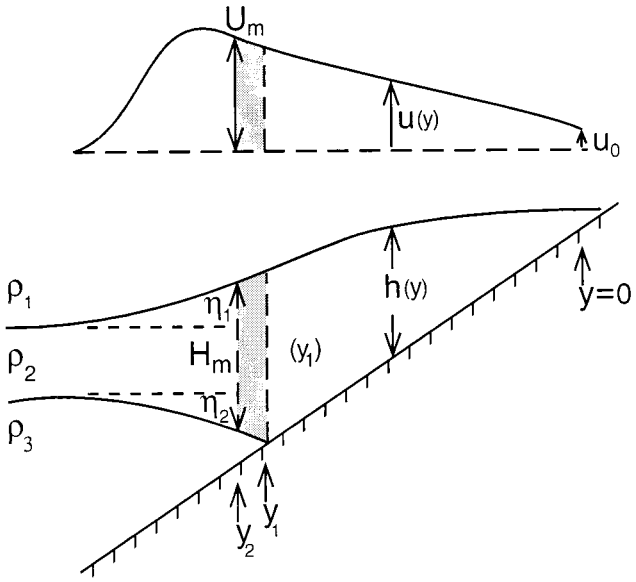

FIG. 2. An idealization (looking downstream) of Fig. 1*B* showing a vertical section (*Lower*) of a jet with downstream velocity $u(y)$ (*Upper*) confined to an intermediate density layer ρ_2; the velocity is assumed to vanish in the overlying ρ_1 layer and the underlying ρ_3 layer. A steady state with slowly varying downstream (not shown) bottom slope $[r(x)]$ forces corresponding offshore displacements of fluid columns, as indicated by the shaded column ($y_2 > y > y_1$), which was located over the bottom slope in the upstream region ($x = -\infty$, not shown). The $y = 0$ origin at any x-section is taken at the front where the layer thickness $h(y)$ vanishes. Although the corresponding velocity u_0 also vanishes in the assumed *upstream* state, the *inviscid* theory used must allow $u_0 \geq 0$ at downstream x. See text.

irregularity of the California coastal topography produces a (nonspatially periodic) baroclinic instability. The net result is that some fluid separates from the main coastal current, forming structures that extend to large offshore distances and resemble the filaments and "squirts" observed in the surface layer of the California Current. Haidvogel *et al*. (11) note, however, that this effect is reduced or suppressed if the variable topography is removed and replaced by a straight vertical wall on the inshore side of an unstable laminar boundary jet.

The foregoing studies suggest that the separation of *intermediate* depth eddies from the Mediterranean outflow is due to a local region of enhanced instability, resulting from some prior influence of slope topography. But the intrinsic complexity of the cited numerical models does not allow us to identify that influence, and, to isolate it, we turn to the following simpler analytical model.

Section 2. Description of the Model

Fig. 2 is a vertical section of a geostrophically balanced jet that is confined to an intermediate density layer ρ_2 lying between two very deep density layers ($\rho_1 < \rho_2$, $\rho_3 > \rho_2$) whose velocity is assumed to vanish everywhere. Thus part of the midlevel (ρ_2) jet is supported by the continental slope, and part is supported by the pressure on the interface of the ρ_3 layer. Far upstream ($x = -\infty$) from Fig. 2 the laminar velocity of the jet is given as a function of the cross-stream distance y; at some downstream position x the bottom slope $r(x)$ starts to increase gradually, thereby forcing cross-stream displacements in the ρ_2 layer. These will be computed by using the inviscid, steady, and shallow water (hydrostatic) equations in a rotating system with constant Coriolis parameter f. Assuming that at $y = \infty$, $\partial h/\partial x \equiv 0$, the resulting nonlinear equations will give, at any x, the downstream velocity $u(y)$ and the total layer thickness $h(y)$. Without loss of generality, the $y = 0$ origin at any downstream section (e.g., Fig. 2) is conveniently taken at the inshore "front" of the ρ_2 density layer where $h(0) = 0$. For physical reasons it is desirable to restrict the theory to the case where $u(0) \equiv u_0 = 0$ in the upstream ($x = -\infty$) state, but the *inviscid* theory must allow for finite positive u_0 further downstream. [It is anticipated that the inclusion of a thin *viscous* layer at the front ($y = 0$) will remove the unrealistic velocity discontinuity across $y = 0$.] However, steady solutions of the longwave equations with *negative* $u(0)$ in the downstream state cannot be admitted, although such an *upstream* influence is physically possible, and it would require a more general theory.

At any downstream x, or at any $r(x)$, let y_1 (Fig. 2) denote the point where the lower interface intersects the slope; the far upstream $[r(-\infty)]$ values of $y_1 = L$, $h(y_1) = H_m$, and $u(y_1) = U_m$ are given. We want to compute the value of $y_1 - L$ when these parameters are such that the streamline originating at $y = L$ is deflected *offshore* (and on to the ρ_3 interface) to $y = y_2 > y_1$.

Since $h(x, \infty)$ is assumed constant, and since the longwave theory implies the balance of Coriolis (fu) and the pressure gradient force, the conservation of volume transport in $y_2(x) \leq y < \infty$ yields the important boundary condition $h(y_2) = H_m$. The Bernoulli invariant then gives $u(y_2) = U_m$ as a second boundary condition for all the fluid in $y_2 \geq y \geq y_1$ (at any x) which originated on the slope at $x = -\infty$. On each such streamline potential vorticity P is conserved, and, to close the problem for this region in the simplest dynamically consistent way, we will assume uniform upstream P in $L > y > 0$, and therefore uniform P in $y_2(x) \geq y \geq 0$. Since the total volume transport Q in this interval is also independent of x, we will obtain (*Section 3*) three (highly) nonlinear *algebraic* equations for $y_1(x)$, $u_0(x)$, and $h(y_1(x))$. But it is easier to solve these equations by differentiating with respect to x (using $dQ/dx = 0$), and then integrating by using a second-order Runge–Kutta scheme to obtain y_1, etc. as a function of $r(x)$.

To quantify the foregoing considerations for the steady flow in $y_2(x) > y_1(x) > y > 0$ we first note that the vanishing velocity in the ρ_1, ρ_3 layers, and the longwave approximation give the downstream *geostrophic* velocity in the ρ_2 layer:

$$u = -\frac{g^*\varepsilon}{f}\frac{\partial h}{\partial y} \qquad y_2 > y > y_1 \qquad \textbf{[2.1]}$$

$$u = -\frac{g^*}{f}\frac{\partial h}{\partial y} + \frac{g^* r}{f}, \qquad y_1 \geq y \geq 0 \qquad \textbf{[2.2]}$$

where

$$g^* = g\Delta_1 \qquad \Delta_1 = (\rho_2 - \rho_1)/\rho_1 \qquad \textbf{[2.3]}$$

$$\varepsilon = \Delta_2/(\Delta_2 + \Delta_1) \qquad \Delta_2 = (\rho_3 - \rho_2)/\rho_2. \qquad \textbf{[2.4]}$$

In $y_2 > y > 0$, the volume transport

$$Q = \int_0^{y_2(x)} uh\, dy \qquad \textbf{[2.5]}$$

is independent of x, and the nondimensional longwave potential vorticity

$$P = \frac{f - \partial u/\partial y}{h(y)}\frac{H_m}{f} \qquad \textbf{[2.6]}$$

is uniform in (x, y). The aforementioned endpoint conditions (for Eq. **2.6**) are

$$h(y_2) = H_m \qquad u(y_2) = U_m, \qquad \textbf{[2.7a]}$$

$$h(0) = 0. \qquad \textbf{[2.7b]}$$

The given nondimensional parameters, in addition to ε, are

$$s(x) \equiv \frac{r(x)g^*}{f^2L} \qquad s_0 = \frac{r(-\infty)g^*}{f^2L}, \qquad \textbf{[2.8a]}$$

$$F^2 \equiv \frac{f^2L^2}{g^*H_m} \qquad q \equiv \frac{Q}{H_mL^2f}, \qquad \textbf{[2.8b]}$$

and the relevant dependent variables are

$$\hat{y} \equiv y_1/L \qquad \hat{h} \equiv \frac{g^*h(y_1)}{f^2L^2} \qquad \hat{u}_0 = u_0/fL. \qquad \textbf{[2.9]}$$

In the upstream state, where s_0 is the nondimensional slope, the endpoint values of **2.9** are

$$\hat{y} = 1 \qquad \hat{h} = 1/F^2, \qquad \textbf{[2.10a]}$$

$$\hat{u}_0 = 0 \qquad \text{(assumed)}. \qquad \textbf{[2.10b]}$$

It is important to note that all of the following considerations are independent of the *detailed* upstream structure of the jet in $y > L$; although the boundary conditions **2.7a** will be used at $y = y_2$, they are only consequences of *integral* properties of the fluid in $y \geq y_2$, as has been pointed out.

Also note that Eq. **2.10b** and the conservation of the Bernoulli function on $y = 0$ require that if $u(0)$ increases downstream, then the elevation of the free streamline relative to a fixed datum level must decrease, and this requires a deflection of slope water to greater depths. The central qualitative question then is whether the slope required for this *inviscid* effect must *increase*, as is tentatively assumed below. The necessary calculations are simplest for the case (*Section 3*) of vanishing potential vorticity Eq. **2.6**, and the quantitative effect of finite P is computed in *Section 4*. The implication for meddy formation as a result of the predicted offshore deflection is discussed in *Section 5*, along with a suggestion for testing the conjecture.

Section 3. Vanishing Inshore Potential Vorticity ($P = 0$)

In this case the solution of **2.6** is the linear velocity profile

$$u = fy + u_0, \qquad y_2 \geq y \geq 0, \qquad \textbf{[3.1a]}$$

where u_0 is an unknown function of x, and the second boundary condition in **2.7a** then gives

$$U_m = fy_2 + u_0. \qquad \textbf{[3.1b]}$$

One equation relating the three unknowns $[y_1, u_0, h(y_1)]$, obtained by integrating **2.2** using **3.1a**, is

$$\frac{g^*h(y_1)}{f} = \frac{g^*ry_1}{f} - \frac{fy_1^2}{2} - u_0y_1. \qquad \textbf{[3.2]}$$

A second equation is supplied by **2.5**, the right-hand side of which equals the sum of

$$\int_{y_1}^{y_2} uhdy = \frac{g^*\varepsilon}{2f}[h^2(y_1) - H_m^2],$$

and

$$\int_0^{y_1} uhdy = \int_0^{y_1} dy\left(\frac{h}{2f}\right)\frac{d}{dy}(fy + u_0)^2$$

$$= \frac{h(y_1)(fy_1 + u_0)^2}{2f} + \left[\frac{1}{2g^*}\int_0^{y_1}(fy + u_0)^3dy - \frac{r}{2f}\int_0^{y_1}(fy + u_0)^2dy\right],$$

where **3.1a** and **2.2** have been used. Thus the given upstream transport equals

$$Q = \frac{g^*\varepsilon}{2f}[h^2(y_1) - H_m^2] + \frac{h(y_1)}{2f}(fy_1 + u_0)^2 + \frac{1}{8g^*f}\{(fy_1 + u_0)^4 - u_0^4\} - \frac{r}{6f^2}\{(fy_1 + u_0)^3 - u_0^3\}. \qquad \textbf{[3.3]}$$

The third and final equation is obtained by using **3.1a** in **2.1**, and by integrating from y_1 to y_2. The right-hand side of the result is $g^*\varepsilon f^{-1}[h(y_1) - H_m]$, and the left-hand side is $\frac{1}{2}[U_m + (fy_1 + u_0)][y_2 - y_1]$. Since **3.1a, b** implies $f(y_2 - y_1) = U_m - (fy_1 + u_0)$, we get

$$\frac{1}{2\varepsilon}[U_m^2 - (u_0 + fy_1)^2] = g^*ry_1 - \frac{f^2y_1^2}{2} - u_0y_1f - g^*H_m, \qquad \textbf{[3.4]}$$

where **3.2** has been used.

By applying **2.8–2.9** and $q \equiv Q/(H_mL^2f)$, the nondimensional forms of Eqs. **3.2–3.4** become

$$\hat{h} = s\hat{y} - \frac{\hat{y}^2}{2} - \hat{u}_0\hat{y} \qquad \textbf{[3.5]}$$

$$\frac{1}{2\varepsilon}[1 - (\hat{u}_0 + \hat{y})^2] = s\hat{y} - \frac{\hat{y}^2}{2} - \hat{u}_0\hat{y} - \frac{1}{F^2} \qquad \textbf{[3.6]}$$

$$q = \frac{\varepsilon F^2\hat{h}^2}{2} - \frac{\varepsilon}{2F^2} + \frac{\hat{h}F^2}{2}(\hat{y} + \hat{u}_0)^2 - \frac{F^2}{8}\{(\hat{y} + \hat{u}_0)^4 - \hat{u}_0^4\} - \frac{F^2s}{6}[(\hat{y} + \hat{u}_0)^3 - \hat{u}_0^3]. \qquad \textbf{[3.7]}$$

From **2.10a, b** it is seen that when **3.5** and **3.6** are evaluated far upstream the result is

$$\hat{h} = s_0 - \tfrac{1}{2}, \qquad \textbf{[3.8a]}$$

$$\frac{1}{F^2} = s_0 - \tfrac{1}{2}. \qquad \textbf{[3.8b]}$$

Note that **3.2** also holds at *all* y, so that in the upstream state ($u_0 = 0$), $\partial h(L^-)/\partial y = 0$ if $g^*r(-\infty)/f - fL = 0$, or if $s_0 = 1$. The latter value therefore occurs when the bottom slope equals the upper density slope of the interface (Fig. 2). Also note that our $P \equiv 0$ model is highly constrained in the parametric sense, since it only allows $s_0 > \frac{1}{2}$ (according to **3.8a**). Moreover, very large values of s_0 are not of interest because they correspond (**3.8b**) to $F \to 0$ or $L \to 0$ (**Eq. 2.8**), in which case the portion of the *upstream* jet lying over the slope is *already* very small; the problem of interest occurs when L is comparable to the radius of deformation $(g^*H_m)^{1/2}/f$, or $F = O(1)$.

As previously stated, the complicated algebraic equations **3.5–3.7** are best solved by first differentiating them with respect to the downstream distance, or with respect to s (denoted by a prime), and using $dq/ds = 0$:

$$\hat{h}' + (\hat{y} - s + \hat{u}_0)\hat{y}' + \hat{y}u_0' = \hat{y} \qquad \textbf{[3.9]}$$

$$[\hat{y} - s + \hat{u}_0 - (\hat{u}_0 + \hat{y})/\varepsilon]\hat{y}' + [\hat{y} - (\hat{u}_0 + \hat{y})/\varepsilon]\hat{u}_0' = \hat{y} \qquad \textbf{[3.10]}$$

$$[\varepsilon\hat{h} + (\hat{y} + \hat{u}_0)^2/2]\hat{h}' + [\hat{h}(\hat{y}_0 + \hat{u}_0) + (\hat{y} + \hat{u}_0)^3/2]\hat{y}' + [\hat{h}(\hat{y} + \hat{u}) + \{\hat{y} + \hat{u}_0)^3 - \hat{u}_0^3\}/2 - s\{(\hat{y} + \hat{u}_0)^2 - \hat{u}_0^2/2\}\hat{u}_0' = ((\hat{y} + \hat{u}_0)^3 - \hat{u}_0^3)/6, \qquad \textbf{[3.11]}$$

where $\hat{y}' = d\hat{y}_1/ds$, etc.

Instructive results for "small" $s - s_0$ are obtained by linearizing about $\hat{u}_0 = 0$, $\hat{y} = 1$, $\hat{h} = 1/F^2$ to get

$$\hat{h}' + (1 - s_0)\hat{y}' + \hat{u}_0' = 1$$

$$\left(1 - s_0 - \frac{1}{\varepsilon}\right)\hat{y}' + \left(1 - \frac{1}{\varepsilon}\right)\hat{u}_0' = 1$$

$$\left(\frac{\varepsilon + F^2}{2}\right)\hat{h}' + \left[1 + \frac{F^2}{2} - \frac{F^2 s_0}{2}\right]\hat{y}' + \left[1 + \frac{F^2}{2} - \frac{F^2 s_0}{2}\right]\hat{u}_0' = \frac{F^2}{6}.$$

The determinant of this system $[s_0F^2(1 - \varepsilon + \varepsilon s_0)/2\varepsilon]$ is positive, since $\varepsilon < 1$, and the explicit solution is

$$\hat{y}' = \frac{\frac{1}{3} - \frac{1}{3\varepsilon} - \frac{s_0}{2}}{(1 - \varepsilon + \varepsilon s_0)/2\varepsilon} < 0 \qquad \textbf{[3.12]}$$

$$\hat{u}_0' > 0. \qquad \textbf{[3.13]}$$

From this we conclude that if the slope increases downstream ($ds = s - s_0 > 0$) then $d\hat{y} = (y_1 - L)/L < 0$ and the fluid is deflected *off*shore; also $d\hat{u}_0 > 0$, verifying that a parcel on the frontal ($y = 0$) free streamline increases its downstream speed. The quantitative result for $\varepsilon = \frac{1}{2}$ and $s_0 = 1$ is

$$\hat{y}' = -5/6. \qquad \textbf{[3.14]}$$

For finite $s - s_0$ we integrate **3.9–3.11** for a given (ε, s_0), starting from $\hat{y} = 1$, $\hat{u}_0 = 0$, $\hat{h} = s_0 - \frac{1}{2}$. Fig. 3 shows the results for $s_0 = 1$ ($F^2 = 2$), $s_0 = \frac{3}{4}$ ($F^2 = 4$), and various $\varepsilon = (\frac{1}{3}, \frac{1}{2}, \frac{2}{3})$. For $s_0 = 1$, $\varepsilon = \frac{1}{2}$ a 4-fold increase in the downstream bottom slope causes 70% of the width of the upstream slope current to be deflected into deep water, where it is sandwiched between the passive ρ_1 and ρ_3 layers. A similar fractional displacement occurs for $\varepsilon = \frac{1}{2}$, $s_0 = 0.75$.

Section 4. Finite Potential Vorticity *P*

If P in Eq. **2.6** is a finite positive constant at all $y_2(x) \geq y \geq 0$, then the solutions for $h(y)$ in each of the two regions (cf. Eqs. **2.1** and **2.2**) are hyperbolic functions. These must be joined to satisfy the continuity of u at the point $y = y_1$ where the lower density interface intersects the bottom (Fig. 1), and where $\partial h/\partial y$ is discontinuous. In solving **2.6** etc., the same nondimensionalization is used as in *Section 3* (see Eqs. **2.8** and **2.10**), and the subsequent procedure is similar to that used in obtaining Eqs. **3.9–3.11**. After considerable algebra the following system of nonlinear differential equations is obtained for $\hat{y}' = d\hat{y}/ds$, etc.:

$$a_{11}\hat{y}' + a_{12}\Delta\hat{y}' + a_{13}\hat{u}_0' = -a_{14} \qquad \textbf{[4.1]}$$

$$a_{21}\hat{y}' + a_{22}\Delta\hat{y}' + a_{23}\hat{u}_0' = -a_{24} \qquad \textbf{[4.2]}$$

$$a_{31}\hat{y}' + a_{32}\Delta\hat{y}' + a_{33}\hat{u}_0' = -a_{34}, \qquad \textbf{[4.3]}$$

where

$$\Delta\hat{y} \equiv (y_2 - y_1)/L. \qquad \textbf{[4.4]}$$

The coefficients $a_{11}, \ldots, a_{34}$ are nonlinear functions of $\hat{y}$, $\Delta\hat{y}$, $\hat{u}_0$, and are listed in the *Appendix*. In addition, these coefficients depend on the upstream parameters (F, s_0, P), which are not independent, but related by

$$\frac{1}{F^2} = \frac{1 - \cosh P^{1/2}}{P} + \frac{s_0 \sinh P^{1/2}}{P^{1/2}}. \qquad \textbf{[4.5]}$$

The Runge–Kutta integration of these equations then proceeds from the upstream values of

$$\hat{y} = 1, \qquad \Delta\hat{y} = 0, \qquad \hat{u}_0 = 0 \qquad \textbf{[4.6]}$$

to any downstream values of s.

The main result (Fig. 4) is similar to that obtained for the much simpler case ($P = 0$), except that the fractional offshore displacement of the slope current is somewhat larger for *finite* potential vorticity. For example, when $P = 1.6$, $F^2 = 4$, and $\varepsilon = 0.5$, the upstream state is given by $s_0 = 0.65$, $y_1/L = 1.0$, and $\hat{u}_0 = 0$. For a downstream $s = 2.6$, we obtain $y_1/L = 0.25$, $\hat{y} = 0.49$. Thus the width of the current in contact with the slope is reduced to one-fourth of its upstream value, and considering that $\hat{h}(0) = 0$ we see that the cross-sectional area of the downstream slope current is very small. It is expected that the inclusion of (Ekman) frictional effects will reduce $\hat{u}_0$ toward zero, causing almost all of the current at the downstream section to lie above the deep ρ_3 layer.

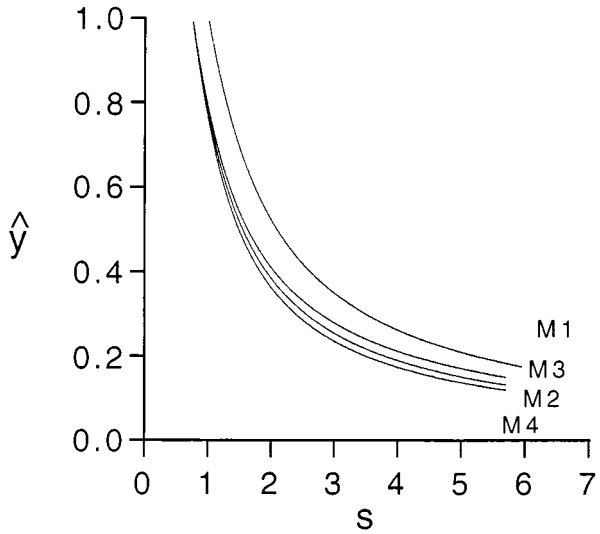

FIG. 3. The fractional width $\hat{y}$ of the upstream current lying above the continental slope that is deflected offshore (cf. Fig. 2) as a function of nondimensional slope $s = \frac{1}{2} + 1/F^2$ when the potential vorticity (P) vanishes. M1: $F^2 = 2$, $\varepsilon = \frac{1}{2}$; M2: $F^2 = 4$, $\varepsilon = \frac{1}{2}$; M3: $F^2 = 4$, $\varepsilon = \frac{1}{3}$; M4: $F^2 = 4$, $\varepsilon = \frac{2}{3}$.

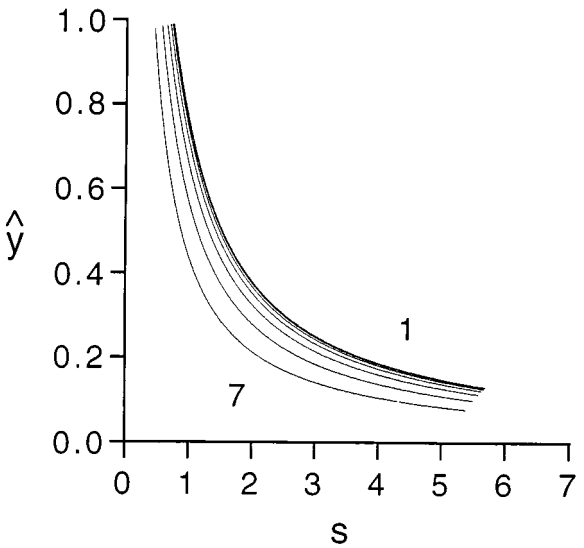

FIG. 4. Same as Fig. 3 except for finite P and ($F^2 = 4$, $\varepsilon = 0.5$). Curves 1–7 are, respectively, $P = 0.1$, $P = 0.2$, $P = 0.4$, $P = 0.8$, $P = 1.6$, $P = 3.2$, and $P = 6.4$.

Section 5. Conclusion and Suggestion

A steady-state finite-amplitude theory has shown that a downstream increase in cross-stream topographic slope (equivalent to gradually convergent isobaths) will deflect a midlevel density current (Fig. 2) away from the continental slope and onto the isopycnal surfaces in the deep ocean. Although complete separation ($y_1/L = 0$) does not occur (Figs. 3 and 4), the expected magnitude ($y_1/L \simeq \frac{1}{4}$) of the effect is such that the baroclinic jet is nearly free of the topographic constraint. It is therefore suggested that a local baroclinic instability of our steady-state solution will occur, amplifying the computed offshore displacement and producing an eddy that eventually detaches seaward of the remaining current on the slope. Obviously, this *time*-dependent scenario for meddy formation is beyond our present scope, but the speculation can be tested by a numerical calculation starting with a completely laminar undisturbed flow (like that in Fig. 2 but with $\partial u/\partial x \equiv 0$), and then imposing a slowly varying downstream slope r. The resulting forced offshore deflection should start out similar to that given by the foregoing theory, except that the *time*-dependent motions induced in the (bottom) ρ_3 layer now become important, and the baroclinic coupling with the motion in the ρ_2 layer may amplify its offshore displacement, causing an anticyclonic eddy in the ρ_2 layer to pinch off from the main current.

Appendix

Tabulation of the coefficients of Eqs. **4.1–4.3**:

$$a_{11} = (1 + \alpha^2)^{1/2}A + \alpha(\varepsilon p)^{-1/2}B$$

$$a_{12} = (p/\varepsilon)^{1/2}\alpha(C - 1/p) + (1 + \alpha^2)^{1/2}\varepsilon^{-1}(D - s)$$

$$a_{13} = -(1 + \alpha^2)^{1/2}p^{-1/2}\sinh(p^{1/2}\hat{y}) - \alpha(\varepsilon p)^{-1/2}\cosh(p^{1/2}\hat{y})$$

$$a_{14} = -a_{13} - \alpha(\varepsilon p)^{-1/2}$$

$$a_{21} = \alpha(p/\varepsilon)^{1/2}A + (1 + \alpha^2)^{1/2}\varepsilon^{-1}B$$

$$a_{22} = (p/\varepsilon)(C - 1/p)(1 + \alpha^2)^{1/2} + (D - s)\alpha(p/\varepsilon)^{1/2}$$

$$a_{23} = -\alpha\varepsilon^{-1/2}\sinh(p^{1/2}\hat{y}) - (1 + \alpha^2)^{1/2}\varepsilon^{-1}\cosh(p^{1/2}\hat{y})$$

$$a_{24} = \alpha\varepsilon^{-1/2}\sinh(p^{1/2}\hat{y}) + (1 + \alpha^2)^{1/2}\varepsilon^{-1}\cosh(p^{1/2}\hat{y}) - (1 + \alpha^2)^{1/2}/e$$

$$a_{31} = s[p^{-1} - p^{-1}\cosh(p^{1/2}\hat{y}) + (s - u_0)p^{-1/2}\sinh(p^{1/2}y) - C(1 - \varepsilon)A$$

$$a_{32} = 0$$

$$a_{33} = -(s/p)[\cosh(p^{1/2}\hat{y}) - 1] + (1 - \varepsilon)p^{-1/2}C\sinh(p^{1/2}\hat{y})$$

$$a_{34} = \hat{y}/p - p^{-3/2}\sinh(p^{1/2}\hat{y}) + (2s - \hat{u}_0)p^{-1}[\cosh(p^{1/2}\hat{y}) - 1] - (1 - \varepsilon)p^{-1/2}C\sinh(p^{1/2}\hat{y})$$

$$A = -p^{1/2}\sinh(p^{1/2}\hat{y}) + (s - \hat{u}_0)\cosh(p^{1/2}\hat{y})$$

$$B = -\cosh(p^{1/2}\hat{y}) + p^{1/2}(s - u_0)\sinh(p^{1/2}\hat{y})$$

$$C = [1 - \cosh(p^{1/2}\hat{y})]/p + (s - \hat{u}_0)p^{-1/2}\sinh(p^{1/2}\hat{y})$$

$$D = -p^{-1/2}\sinh(p^{1/2}\hat{y}) + (s - \hat{u}_0)\cosh(p^{1/2}\hat{y})$$

$$\alpha = \sinh[(p/\varepsilon)^{1/2}\Delta\hat{y}].$$

I thank Dr. Amy Bower (Woods Hole Oceanographic Institution) for discussion of the meddy observations. Part of this research was supported by the National Science Foundation (Grants OCE-9529261 and OCE-9726584).

1. Stern, M. E. (1998) *J. Phys. Oceanogr.* **28,** 2040–2049.
2. Olson, D. B., Brown, O. B. & Emmerson, S. R. (1983) *J. Geophys. Res.* **88** (C8), 4569–4577.
3. Bower, A. B., Armi, L. & Ambar, J. (1997) *J. Phys. Oceanogr.* **27,** 2545–2575.
4. D'Asaro, E. A. (1988) *J. Geophys. Res.* **93** (C6), 6669–6884.
5. D'Asaro, E. A. (1988) *J. Geophys. Res.* **93** (C6), 6685–6697.
6. Klinger, B. A. (1994) *J. Phys. Oceanogr.* **24,** 1805–1811.
7. Klinger, B. A. (1994) *J. Geophys. Res.* **99** (C6), 12515–12531.
8. Jiang, L. & Garwood, R. W. (1998) *J. Geophys. Res.* **103** (C3), 5459–5476.
9. Allen, J. S., Walstad, L. J. & Newberger, P. A. (1991) *J. Geophys. Res.* **96** (C8), 14995–15016.
10. Käse, R. H., Beckmann, A. & Hinrichsen, H. H. (1989) *J. Geophys. Res.* **94** (C4), 4905–4912.
11. Haidvogel, D. B., Beckmann, A. & Hedström, K. S. (1991) *J. Geophys. Res.* **96** (C8), 15017–15040.